



HAL
open science

Low temperature oxygen diffusion mechanisms in $\text{Nd}_2\text{NiO}_{4+\delta}$ and $\text{Pr}_2\text{NiO}_{4+\delta}$ via large anharmonic displacements, explored by single crystal neutron diffraction

Monica Ceretti, Olivia Wahyudi, Alain Cousson, Antoine Villesuzanne, Martin Meven, Bjørn Pedersen, Jean-Marc. Bassat, Werner Paulus

► To cite this version:

Monica Ceretti, Olivia Wahyudi, Alain Cousson, Antoine Villesuzanne, Martin Meven, et al.. Low temperature oxygen diffusion mechanisms in $\text{Nd}_2\text{NiO}_{4+\delta}$ and $\text{Pr}_2\text{NiO}_{4+\delta}$ via large anharmonic displacements, explored by single crystal neutron diffraction. *Journal of Materials Chemistry A*, 2015, 3 (42), pp.21140-2148. 10.1039/c5ta05767a . hal-01229929

HAL Id: hal-01229929

<https://hal.science/hal-01229929>

Submitted on 5 Feb 2021

HAL is a multi-disciplinary open access archive for the deposit and dissemination of scientific research documents, whether they are published or not. The documents may come from teaching and research institutions in France or abroad, or from public or private research centers.

L'archive ouverte pluridisciplinaire **HAL**, est destinée au dépôt et à la diffusion de documents scientifiques de niveau recherche, publiés ou non, émanant des établissements d'enseignement et de recherche français ou étrangers, des laboratoires publics ou privés.

Low temperature oxygen diffusion mechanisms in $\text{Nd}_2\text{NiO}_{4+\delta}$ and $\text{Pr}_2\text{NiO}_{4+\delta}$ via large anharmonic displacements, explored by single crystal neutron diffraction

M. Ceretti,^{*a} O. Wahyudi,^{†bcd} A. Cousson,^e A. Villesuzanne,^{bcf} M. Meven,^{ghi} B. Pedersen,^g J. M. Bassat^{bc} and W. Paulus^a

^a Institut Charles Gerhardt Montpellier, UMR 5253 CNRS-Université de Montpellier, Chimie et Cristallographie des Matériaux, Place Eugène Bataillon, 34095 Montpellier, France

^b CNRS, ICMCB, UPR 9048, F-33600 Pessac, France

^c Univ. Bordeaux, ICMCB, UPR 9048, F-33600 Pessac, France

^d Sciences Chimiques de Rennes, Université de Rennes 1, France

^e Laboratoire Léon Brillouin, UMR 12 CEA-CNRS, Gif sur Yvette, 91191 France

^f IREET, University of Bolton, Bolton, UK

^g Heinz Maier-Leibnitz Zentrum (MLZ), Technische Universität München, 85747 Garching, Germany

^h RWTH Aachen University, Institut für Kristallographie, Outstation at MLZ, Germany

ⁱ FZ Jülich GmbH, Jülich Centre for Neutron Science JCNS, Outstation at MLZ, 85747 Garching, Germany

* Corresponding authors / E-mail: monica.ceretti@univ-montp2.fr

Footnote :

† Present address: Shanghai Institute of Ceramics, Chinese Academy of Sciences, 1295 Dingxi Road, Shanghai, P. R. China 200050.

Abstract: We investigated the structure of $\text{Nd}_2\text{NiO}_{4+\delta}$ and $\text{Pr}_2\text{NiO}_{4+\delta}$ by single crystal neutron diffraction studies. While the real structure of both compounds is incommensurate, the scattering density of the respective average structures was explored using the Maximum Entropy Method. Unusually high displacement factors were found for the equatorial and apical oxygen atoms showing respectively large displacement amplitudes towards [001] and [110] with respect to the F-symmetry cell. The shifts of the apical oxygen atoms reach up to 1 Å from their average position, corresponding to a 25° tilt of the NiO_6 octahedra. At 400 °C, *i.e.* slightly above the orthorhombic-tetragonal phase transition, the anharmonic apical oxygen displacements towards [110] in the commensurate tetragonal parent structure are strongly enhanced, showing a double-well potential and pointing towards the interstitial vacancy sites, creating a quasi continuous shallow energy diffusion pathway between apical and interstitial oxygen sites. These large displacement amplitudes are considered to be – at least partially – of dynamical origin, which is consistent with a phonon assisted diffusion mechanism, already activated at very moderate temperatures.

Introduction

Understanding fundamental aspects of oxygen diffusion in solid oxides at moderate temperatures, down to ambient, is an important issue for the development of a variety of technological devices in the near future. This concerns *e.g.* the progress and invention of next generation solid oxygen ion electrolytes and oxygen electrodes for solid oxide fuel cells (SOFCs) as well as membrane based air separators, oxygen sensors and catalytic converters to transform *e.g.* NO_x or CO from exhaust emissions into N_2 and CO_2 .^{1–5} Taking the example of SOFCs, which combine highly efficient energy conversion of fossil and non-fossil fuels (*e.g.* H_2), the main drawback of long-term endurance is related to the relatively high operating temperature of around 1000–1250 °C, presenting a key challenge in terms of fatigue due to compositional and microstructural degradation of the respective electrode/membrane materials. Accordingly, huge efforts are currently undertaken to develop suitable materials, allowing a considerable lowering of the operating temperatures down to below 800 °C, while preserving high oxygen diffusion rates. Bulk oxygen ion diffusion strongly depends on

the temperature, thus lowering the operation temperature directly reduces the oxygen conductivity. In order to optimise solid oxide electrolytes we need, still today, a better fundamental understanding of the diffusion process on a microscopic scale.

Two families of oxides are known today to undergo oxygen intercalation reactions under ambient conditions: the K_2NiF_4 and the Brownmillerite frameworks such as $RE_2MO_{4+\delta}$ ($RE = La, Nd, Pr, M = Cu, Ni, Co$) and $SrMO_{2.5}$ ($M = Fe, Co$),^{6–16} respectively.

Oxygen ion mobility in Brownmillerite phases like $SrFeO_{2.5}$ has been recently evidenced to rely essentially on low energy phonon modes, especially at moderate temperatures.¹⁷ This result gave evidence for the first time to a phonon-assisted diffusion mechanism of the oxygen ions. A similar mechanism could be extended to $La_2CuO_{4.07}$, underlining its more general nature and applicability to K_2NiF_4 type oxides.¹⁸ This is at first sight surprising, as the nature of the vacancies in both types of oxides is different: the Brownmillerite structure has regular vacancy sites, while only interstitial vacancy sites exist in K_2NiF_4 type oxides.

For some K_2NiF_4 -type phases the amount of intercalated oxygen becomes important, and the highest values were found for $La_2CoO_{4+\delta}$ as well as $(Nd/Pr)_2NiO_{4+\delta}$ with $\delta_{max} = 0.25$.^{19,20} This oxygen uptake formally goes along with changes in the valence state of the 3d metal atom, which for $\delta = 0.25$ yields an equal amount of M^{2+}/M^{3+} , modifying physical properties, *e.g.* magnetic interactions. The correlation of changes in the crystal structure and associated lattice dynamics, as a function of the oxygen stoichiometry, are important input parameters for theoretical studies, to access diffusion pathways and activation energies. It has been shown recently that, even if the basic structure of K_2NiF_4 type oxides is rather simple, their description becomes very complex on varying the oxygen content δ , showing charge and/or orbital ordering on a large scale.²¹ For some of these K_2NiF_4 type oxides like $Nd_2NiO_{4+\delta}$ and $Pr_2NiO_{4+\delta}$, additional reflections with respect to the basic structure have been observed by neutron powder diffraction studies;²² these reflections are still today not well understood.

In the last decade, $(Nd/Pr)_2NiO_{4+\delta}$ phases have attracted much attention as promising materials, providing high oxygen mobility already at moderate temperatures, suitable for membranes in next generation SOFCs. Contrary to $La_2(Cu/Ni)O_{4+\delta}$, which releases the extra oxygen at lower temperatures than the operating one for SOFCs, $(Nd/Pr)_2NiO_{4+\delta}$ phases show a higher thermal stability with respect to δ . This enables the study of the interplay of interstitial and apical oxygen atoms together with structural and lattice dynamic modifications, which are important factors with respect to diffusion mechanisms at elevated temperatures.

We were recently able, from neutron time-of-flight spectroscopy experiments coupled with *ab initio* molecular dynamics calculations on $Nd_2NiO_{4+\delta}$ phases, to evidence that excess oxygen at interstitial lattice sites activates large displacements of the apical oxygen atoms along the [110] direction, thus favoring their diffusion towards interstitial sites within the rock-salt layer, already at ambient temperature. A dynamical delocalisation of apical oxygen atoms along [110], strongly stimulated by lattice dynamics, has been confirmed to be a prerequisite for oxygen ion diffusion in K_2NiF_4 type oxides at room temperature.²³ Based on these simulations, we were interested in more accurate analysis of oxygen displacement factors in $Pr_2NiO_{4+\delta}$ and $Nd_2NiO_{4+\delta}$ related to oxygen doping on interstitial sites, which is supposed to induce phonon assisted oxygen diffusion at moderate temperatures, similar to what has been found for $La_2CuO_{4.07}$.¹⁸ To achieve this, we explored temperature dependent high resolution single crystal neutron diffraction studies combined with data analysis using the Maximum Entropy algorithm.

A special focus was set on how the interstitial oxygen stoichiometry for high δ values ($\delta \approx 0.25$) correlates with the apical oxygen displacements and related diffusion pathways towards the interstitial oxygen sites.

Experimental section

Single crystal growth

Large high quality $\text{RE}_2\text{NiO}_{4+\delta}$ (RE = Nd, Pr) single crystals have been obtained by the travelling solvent floating zone method (TSFZ) and were characterised as reported elsewhere.²⁴ The overall oxygen stoichiometry of the as grown crystals, as determined by thermogravimetric analysis, was found to be $\text{Pr}_2\text{NiO}_{4.22(2)}$ and $\text{Nd}_2\text{NiO}_{4.23(2)}$ which we assign in the following to PNO and NNO, respectively.

Neutron diffraction

The average nuclear structures of the as grown single crystals of $\text{Pr}_2\text{NiO}_{4+\delta}$ and $\text{Nd}_2\text{NiO}_{4+\delta}$ were investigated by single crystal neutron diffraction on different neutron 4-circle diffractometers equipped with a point detector (5C2@LLB at the ORPHEE reactor in Saclay, France, and HEiDi@MLZ at the FRM II reactor in Garching, Germany), as well as a 2D-detector (RESI@MLZ at the FRM II reactor in Garching). All three diffractometers have sufficiently short wavelengths ($\lambda = 0.83 \text{ \AA}$ for 5C2, $\lambda = 0.793 \text{ \AA}$ for HEiDi and 1.15 \AA for RESI), to explore the reciprocal space up to high momentum transfers. Structure refinements were carried out using Shelxl²⁵ and nuclear densities were reconstructed in real space through the Maximum Entropy Method (MEM) *via* PRIMA (Practice Iterative MEM Analysis);²⁶ scattering lengths were taken from [ref. 27](#). Nuclear density distributions were visualized by using the VESTA program.²⁸

Results and discussion

Nuclear structure from single crystal neutron diffraction

The diffractometers, 5C2 and HEiDi, have both short wavelengths, allowing an excellent data quality up to high values in $\sin \vartheta/\lambda$ and better exploration of anisotropic and anharmonic displacement parameters, especially for light atoms such as oxygen. As reported elsewhere,²⁴ NNO and PNO single crystals are twinned, with up to four twin individuals, and show a complex incommensurate modulated structure.

[Fig. 1](#) shows the reconstructed ($hk4$) layer of NNO obtained on RESI. Strong contributions of incommensurate reflections, which can be indexed assuming a 2D modulation vector being $\mathbf{q}_1 = (0.4378, -0.2302, 0)$ and $\mathbf{q}_2 = (0.4378, 0.2302, 0)$, become evident in addition to the basic reflections. Their intensities are significant and reach more than 5% compared to the basic reflections, suggesting strong structural modulations. A similar incommensurate structure scheme has been reported recently for $\text{La}_2\text{CoO}_{4+\delta}$, underlying the more general character of complex structural oxygen ordering in K_2NiF_4 -type oxides as a function of δ .²⁹

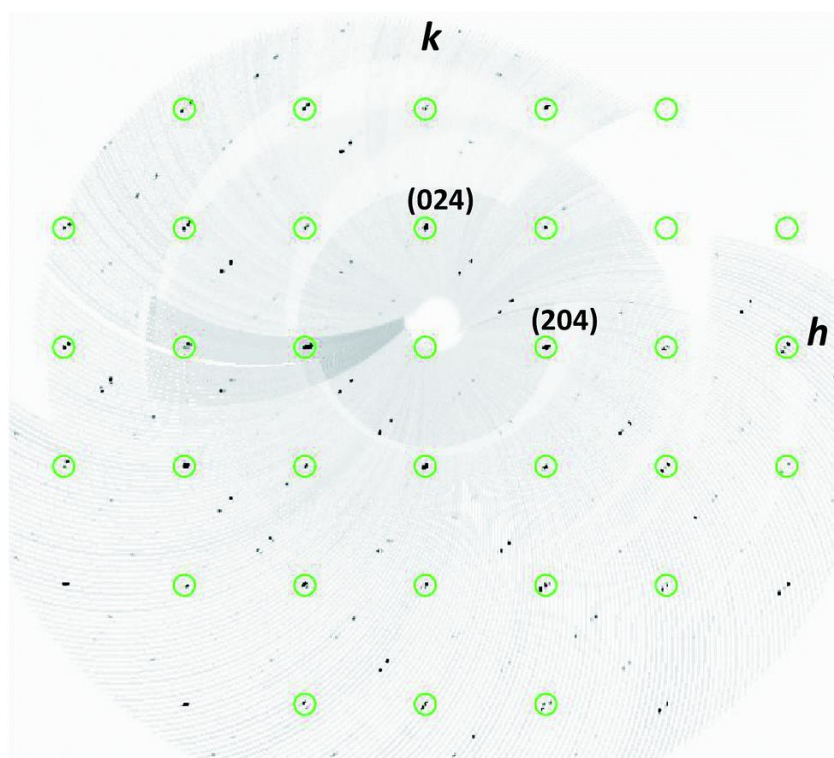


Fig. 1 Reconstructed $(hk4)$ -plane, obtained by neutron diffraction on RESI@MLZ from a $\text{Nd}_2\text{NiO}_{4.25}$ twinned single crystal showing Bragg reflections from two twin individuals. Strong incommensurate reflections are observed in addition to the basic reflections (green circles), which indexation is given with respect to the average $F4/mmm$ -cell. Note that the real symmetry is still orthorhombic, as can be seen from the characteristic splitting of the basic reflections. The incommensurate reflections can be indexed with a 2D modulation vector with $\mathbf{q}_1 = (0.4378, -0.2302, 0)$ and $\mathbf{q}_2 = (0.4378, 0.2302, 0)$.

Even though the real structure of NNO and PNO is expected to be quite complex, especially with respect to the oxygen positions and thus needing a more sophisticated data analysis, we attempted a first approach towards the average structure of both compounds by single crystal neutron diffraction. Structure factors of all basic reflections were collected up to high q -values, *i.e.* up to $\sin \vartheta/\lambda = 0.89 \text{ \AA}^{-1}$ for NNO and $\sin \vartheta/\lambda = 0.87 \text{ \AA}^{-1}$ for PNO. The fact that both crystals were twinned results in an averaging of (hkl) and (khl) reflections of the different twin individuals. The refinements were consequently done in the average space group $F4/mmm$ (equivalent to the standard space group $I4/mmm$). No absorption correction was applied due to the negligible absorption coefficients of both compounds.

The Lorentz corrected data were refined using anisotropic individual Debye–Waller displacement factors for all atoms, except for the interstitial oxygen atoms refined isotropic, related to their weak occupation density. All refinements were carried out, fixing the occupation of Nd/Pr and Ni to be stoichiometric, while all oxygen occupancies were refined unconstrained, including the interstitial oxygen atoms at $(1/4, 1/4, 1/4)$. Structural data of the average structure in $F4/mmm$ are summarized in [Table 1](#). The tetragonal symmetry for structure refinement was chosen due to the twinning, averaging the integrated intensities of (hkl) and (khl) reflections of the two twin components. The averaging of (hkl) and (khl) intensities is also justified as the volume fractions of the individuals were determined to be close to 50%, yielding badly manageable correlations for refinement, taking into account the twinning. This is especially justified as only F-type reflections, *i.e.* reflections of the average structure and no superstructure reflections are used, showing only slight deviations between (hkl) and (khl) . The resulting phased F_{obs} data were subsequently used for Maximum Entropy reconstruction. Note that the real symmetry is orthorhombic (space group $Fmmm$, not taking into

account the incommensurate reflections) and that the data presented here correspond to the respective average structures.

Table 1 $\text{Pr}_2\text{NiO}_{4+\delta}$ and $\text{Nd}_2\text{NiO}_{4+\delta}$ structure data obtained from single crystal neutron diffraction data, collected on a diffractometer 5C2@LLB with $\lambda = 0.83 \text{ \AA}$, installed at the hot source of the ORPHEE reactor. Refinements have been carried out in space group $F4/mmm$

Atom	x	y	z	occ	U_{11}	U_{22}	U_{33}	U_{12}
$\text{Pr}_2\text{NiO}_{4+\delta}$^a								
Pr	0	0	0.3601(4)	2.00	0.010(1)	0.010(1)	0.009(2)	
Ni	0	0	0	1.00	0.0016(7)	0.0016(7)	0.0129(11)	
O _{ap}	0	0	0.1745(4)	1.72(6)	0.046(3)	0.046(3)	0.007(2)	
O _{eq}	1/4	1/4	0	1.96(5)	0.005(4)	0.005(4)	0.038(2)	-0.002(1)
O _{int}	1/4	1/4	1/4	0.245(41)	0.024(9)			
$\text{Nd}_2\text{NiO}_{4+\delta}$^b								
Nd	0	0	0.3592(1)	2.00	0.0147(6)	0.0147(6)	0.0062(7)	
Ni	0	0	0	1.00	0.0071(6)	0.0071(6)	0.00138(8)	
O _{ap}	0	0	0.1723(4)	1.69(6)	0.085(5)	0.085(5)	0.005(2)	
O _{eq}	1/4	1/4	0	2.06(5)	0.013(1)	0.013(1)	0.059(3)	-0.004(1)
O _{int}	1/4	1/4	1/4	0.19(4)	0.014(8)			

^a Orthorhombic lattice parameters: $a = 5.39602(7) \text{ \AA}$, $b = 5.45259(7) \text{ \AA}$, $c = 12.4402(2) \text{ \AA}$ (determined from XRPD, CuK α 1), 263 measured reflections ($\sin \theta/\lambda = 0.87 \text{ \AA}^{-1}$), (155 unique) $R_{\text{int}}(hkl) = 2.17\%$, $R_{\text{(F)}} = 6.55\%$, $R_w = 5.1\%$, U_{ij} in Å^2 . ^b Orthorhombic lattice parameters: $a = 5.37063(4) \text{ \AA}$, $b = 5.45583(4) \text{ \AA}$, $c = 12.3652(1) \text{ \AA}$ (determined from XRPD, CuK α 1), 863 measured reflections ($\sin \theta/\lambda = 0.89 \text{ \AA}^{-1}$), (186 unique) $R_{\text{int}}(hkl) = 6.21$, $R_{\text{(F)}} = 7.54\%$, and $R_w = 6.34\%$, U_{ij} in Å^2 .

Principal difficulties arise for the description of the apical and equatorial oxygen atoms, as strong anisotropic displacement factors were found for both compounds. While the equatorial oxygen atoms show extended/main components of shifts along the c -axis, the apical oxygen atoms are displaced in the a/b -plane. The disorder of the apical oxygen atoms did not allow refining their occupancies within a harmonic description to what would be expected from the crystallographic site multiplicity; for both PNO and NNO single crystals, the refined scattering densities for the oxygen atoms in $(0, 0, z)$ with $z \approx 0.17$ are found in both cases to be about 15% less with respect to a full site occupation. The refinement can be slightly improved when adding partial occupation densities in (x, x, z) with $x \approx 0.09$ and $z \approx 0.175$, but still does not yield *in fine* a full occupation for the apical oxygen site. We underline that this is not related to any oxygen under-stoichiometry, but rather to the fact that the displacements are found to be strongly anharmonic already at ambient T .

This goes along with the fact that the oxygen displacement factors are, on an absolute scale, strongly enhanced compared to what is usually encountered for oxygen intercalated K_2NiF_4 type oxides: the U_{ij} displacement parameters for the apical and equatorial oxygen atoms of NNO and PNO are about 2–3 times larger than found for other $\text{La}_2\text{MO}_{4+\delta}$ phases ($M = \text{Cu}, \text{Ni}, \text{Co}$).³⁰

Of particular interest is whether the strong delocalization of the apical oxygen atoms is of static or dynamical origin, since phonon-assisted oxygen diffusion has been proposed recently for $\text{La}_2\text{CuO}_{4.07}$, showing a similar oxygen disorder scenario. In this context it would be interesting to see if the enhancement of the oxygen mobility is correlated with the amount of interstitial oxygen atoms. This would especially have significant impact on the operation conditions of NNO and PNO oxygen membranes, as both show values of $\delta > 0.15$, even at temperatures above $600 \text{ }^\circ\text{C}$ in air.

Nuclear density maps, obtained from scattering density reconstructions, are of utmost importance to analyse displacements and thus the oxygen disorder scenario. In order to get a quasi model-free description of the nuclear oxygen scattering densities, we subjected all NNO and PNO diffraction data to the Maximum Entropy Method (MEM) algorithm. This approach has the advantage to consider strong and weak reflections with equal importance, resulting in a much better defined background compared to the classical Fourier-methods.

In addition, the MEM algorithm also yields an anharmonic description of the scattering densities, the only constraint to describe scattering densities being imposed by the symmetry of the used space group.³¹ Fig. 2 shows the 3D isosurfaces of the nuclear densities of the NiO₆ octahedra in NNO (Fig. 2a) and PNO (Fig. 2b), as obtained by MEM reconstruction of single crystal neutron diffraction data (5C2@LLB, ORPHEE reactor Saclay) at ambient temperature. Equatorial and apical oxygen atoms are strongly disordered, showing huge anisotropic displacement parameters. In both cases, the isosurfaces of the apical oxygen atoms evidence libration modes along the [110] direction of the F-centred unit cell, modes that are sharper for NNO.

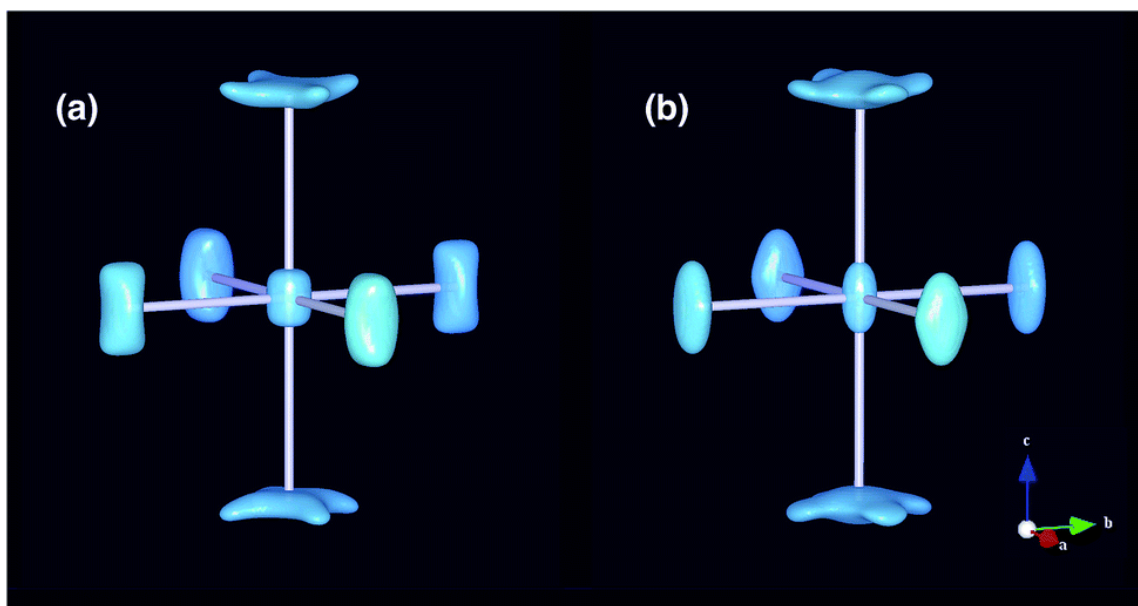


Fig. 2 Representation of the NiO₆ octahedra in NNO (a) and PNO (b) obtained from Maximum Entropy reconstruction of single crystal neutron diffraction data (5C2@LLB, ORPHEE reactor Saclay) at room temperature. Equatorial and apical oxygen atoms are strongly disordered showing huge anisotropic displacement parameters. The isosurfaces of the apical oxygen atoms evidence libration modes along the [110] direction of the F-centred unit cell, modes that appear to be sharper for NNO.

Fig. 3 shows different structural sections of NNO and PNO obtained by MEM reconstruction. While the Ni–O plane at $z = 0$ shows reasonable displacement factors for both compounds as projected on the (a, b) -plane, the sections $0.14 \leq z \leq 0.28$ reveal a more complex situation, especially for the apical oxygen atoms. The apical oxygen disorder scenario of NNO/PNO and especially their strong shifts towards the [110] direction (with respect to the $F4/mmm$ unit cell), corresponds to what is found for La₂CoO_{4.14} at 177 °C, *i.e.* just above the phase transition from the so-called LTO to HTT phases.²⁹ One may suppose these strong apical oxygen displacement factors to be a direct consequence of the incommensurate structural modulation, summarizing on an average scale all deviations of the oxygen atoms from their average position.

At RT the apical oxygen scattering densities correspond, for both compounds, to an anisotropic libration mode in the (a, b) -plane and specifically along [110], on an outer perimeter of about 2 Å. This corresponds to a tilt angle of the NiO₆ octahedron of about 25°, while the extensions are much broader for PNO than for NNO. It becomes obvious that the large amplitudes of the apical oxygen atoms, pointing towards the adjacent interstitial sites, generate a low energy diffusion pathway between these two sites (lower part of Fig. 3). Since the [110] displacements of the apical oxygen atoms reach almost 1 Å, corresponding to half of the diffusion pathway towards the interstitial sites,

one may presume these displacements to be dynamically activated, and consequently to allow significant oxygen mobility for both title compounds.

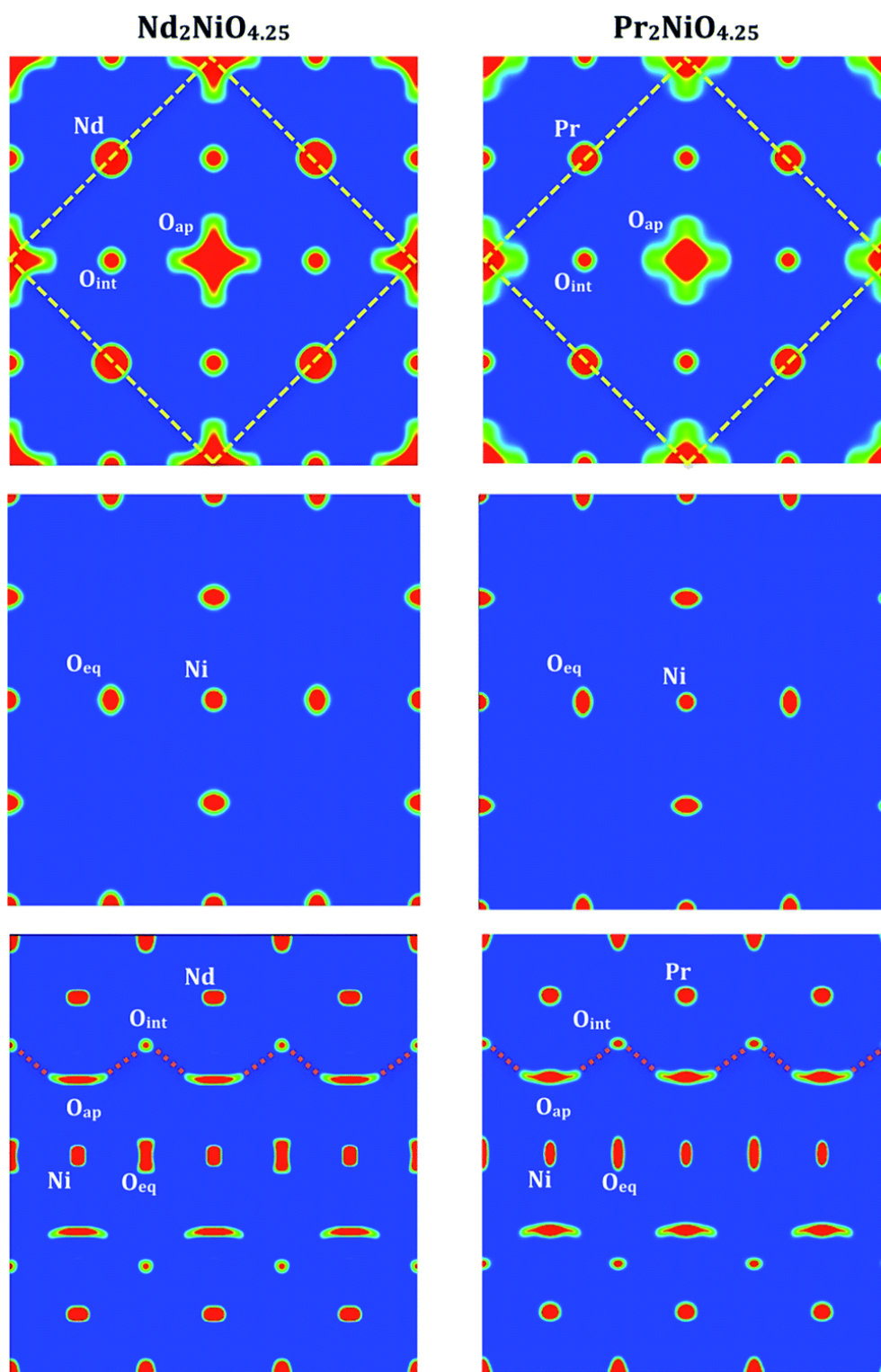


Fig. 3 Nuclear densities of NNO (left) and PNO (right), obtained from neutron single crystal diffraction data via MEM analysis at ambient temperature. Upper and middle part: $2a \times 2a$ projection of the $I4/mmm$ unit cell (the F -centred cell is outlined by yellow dashed bars) from $z = 0.12$ to $z = 0.28$ (upper), thus showing half of the $(Nd/Pr)_2O_2$ rock salt-type layer with positions of the Nd/Pr , apical oxygen and interstitial oxygen atoms at $z = 0.14$, 0.17 and 0.25 , respectively. In the middle part, the NiO plane is given for comparison from $z = -0.08$ to $z = 0.08$. Lower part: $3a \times c$ projection from $y = 0.45$ to $y = 0.55$ in $I4/mmm$. A dashed red line indicates the oxygen diffusion pathways along the a -axis in the I -cell, equivalent to $[110]$ -direction in the F -cell, between apical and interstitial sites.

The strong displacements of the apical oxygen atoms towards [110], as demonstrated in the lower part of Fig. 3 ($3a \times c$ projection), point directly their outer branches towards the interstitial oxygen sites, strongly favouring an interstitial diffusion mechanism, as the O_{ap} displacements are related to the presence and steric pressure of the interstitial oxygen atoms.³² The libration mode of the NiO_6 octahedra can thus not be treated as a rigid body movement, since the curvature of the apical oxygen atom scattering density follows the opening of an inverted umbrella with respect to the central Ni atom (see lower part of Fig. 3).

From the scattering densities of the equatorial oxygen atoms, one may extrapolate a double-well potential established for NNO, while PNO shows a more uniform distribution. This may imply a less activated dynamics for NNO compared to PNO, and may be a hint to explain the different reactivity in terms of electrochemical oxygen intercalation for both compounds. In this context we note that $Pr_2NiO_{4+\delta}$ can take up oxygen reversibly in the range $0 \leq \delta \leq 0.25$; $Nd_2NiO_{4.25}$ can in fact be reduced electrochemically to the stoichiometric (and ambient antiferromagnetically ordered) Nd_2NiO_4 , while its re-oxidation is not fully reversible, and ceases at around $Nd_2NiO_{4.10}$.¹⁶ Also, since the radius of the RE atoms plays an important role in the apical oxygen delocalization, even the small difference existing between Pr^{3+} and Nd^{3+} radii (1.179 Å vs. 1.163 Å, respectively³³) may be sufficient to limit the re-oxidation of $Nd_2NiO_{4.0}$ to a maximum value of $\delta = 0.1$.

An interesting point here is the interstitial oxygen atom position, which came out to be located by the Maximum Entropy reconstruction at exactly (1/4, 1/4, 1/4) and not (1/4, 1/4, 1/4 ± δ) reported elsewhere,³⁴ which goes along with a symmetrically opened $O_{int}(O_{ap})_4$ tetrahedron. These findings are not related to possible artefacts coming from the higher symmetry ($F4/mmm$ rather than the real symmetry $Fmmm$ at ambient T) used for the refinements. This gets especially confirmed from the refinement at 400 °C, for which a tetragonal symmetry also accounts in reality.

Since the presence of one interstitial oxygen atom induces the displacement of four adjacent apical oxygen atoms, both title compounds with δ close to 0.25 exhibit displacements from their average position for half of all apical oxygen atoms. In this way, $\delta = 0.25$ might be interpreted as the upper limit of inserted oxygen stoichiometry, as a further increase of δ will no longer allow a symmetric expansion of *hitherto* unoccupied $O_{int}(O_{ap})_4$ tetrahedra. While all $O_{int}(O_{ap})_4$ tetrahedra are to be expanded, the remaining oxygen vacant tetrahedra should all get downsized. In this way one can also easily understand that the O_{int} stoichiometry around $\delta = 0.25$ should entail strong structural correlations between these different types of tetrahedra, directly related to steric constraints, which obviously also influence the tilting pattern of the NiO_6 octahedra.

For PNO and NNO the apical oxygen displacements related to the symmetric increase of the $O_{int}(O_{ap})_4$ tetrahedron goes along with $O_{int}-O_{ap}$ distances of around 2.8 Å, instead of 2.15 Å for the non-distorted tetrahedron. Such strong local structural distortions also confirm the valence state of all involved oxygen atoms to be essentially O^{2-} , from the almost corresponding sum of the ionic radii of 2 oxygen atoms. This is consistent with our previous DFT investigation of $La_2NiO_{4.25}$: the partition of the calculated electron density, using R. W. Bader's "Atoms in Molecules" scheme, led unambiguously to O^{2-} species for all oxygen ions in this compound, with no significant departure from O^{2-} even in the $O_{int}(O_{ap})_4$ tetrahedra.³⁵

As mentioned above, note that first-principles calculations of zone-center phonon modes in $La_2CuO_{4+\delta}$ showed that the presence of interstitial oxygen atoms induces a shift from [100] to [110] for low-energy apical oxygen libration modes with respect to the F-cell, indicating another indirect role of interstitial oxygen in the diffusion mechanisms. The same type of phonon reorientation behaviour is expected to increase for PNO and NNO as a result of the shortened c -axis.

The oxygen diffusion pathways between apical and interstitial sites have also been simulated by classical methods for $\text{Pr}_2\text{NiO}_{4+\delta}$ above 527 °C, *i.e.* in its HTT phase, and experimentally evidenced from NPD in $(\text{Pr}_{0.9}\text{La}_{0.1})_2(\text{Ni}_{0.74}\text{Cu}_{0.21}\text{Ga}_{0.05})\text{O}_{4+\delta}$ at 1015 °C.^{36,37} This implies a predominantly 2D interstitial diffusion mechanism, as was predicted from MD simulations. Experimental values obtained by isotope exchange depth profiling of oriented single crystals show diffusion coefficients of $1 \times 10^{-7} \text{ cm}^2 \text{ s}^{-1}$ in the (a, b) -plane at 650 °C, while the simulated values from MD³⁶ are exactly of the same order of magnitude. The diffusion coefficients along the c -axis were experimentally found to be at least 3 orders of magnitude lower.³⁸

In this context we were interested to know to what extent the oxygen disorder scenario would change with the incommensurate-commensurate phase transition, taking place at 360 ± 5 °C for PNO as determined for the as grown crystal by neutron diffraction, while the orthorhombic ($Bmab$) to tetragonal ($I4/mmm$) phase transition for stoichiometric Pr_2NiO_4 has been predicted to take place at around 1300 ± 100 °C.³⁹ We observed that all superstructure reflections vanish above 360 °C and that the symmetry changes from orthorhombic to tetragonal. Neutron single crystal data collection of the as grown PNO crystal was carried out at 400 °C on HEiDi@MLZ and the phased data, resulting from the structure refinement in $F4/mmm$ (see [Table 2](#)), were subsequently used for Maximum Entropy reconstruction. The as obtained scattering densities are presented in [Fig. 4](#) and [5](#).

Table 2 $\text{Pr}_2\text{NiO}_{4+\delta}$ structural data obtained at 400 °C in air from single crystal neutron diffraction data, collected on a diffractometer HEiDi@MLZ with $\lambda = 0.793$ Å, installed at the hot source of an FRM II reactor. Refinements were carried out in space group $F4/mmm$ ^a

Atom	x	y	z	occ	U_{11}	U_{22}	U_{33}	U_{12}
Pr	0	0	0.3601(5)	2.00	0.022(2)	0.022(1)	0.020(3)	
Ni	0	0	0	1.00	0.0086(15)	0.0086(15)	0.033(2)	
O _{ap}	0	0	0.1754(6)	2.00	0.075(6)	0.075(6)	0.024(3)	
O _{eq}	1/4	1/4	0	2.00	0.016(2)	0.016(2)	0.059(4)	
O _{int}	1/4	1/4	1/4	0.34(6)	0.05			-0.007(1)

^a Averaged tetragonal lattice parameters: $a = b = 5.460(7)$ Å, $c = 12.586(5)$ Å (determined on HEiDi from 19 centred reflections), 257 measured reflections ($\sin \theta/\lambda = 0.81 \text{ \AA}^{-1}$), (155 unique) $R_{\text{int}}(hkl) = 3.13$, $R_{\text{F}} = 5.85\%$, $R_w = 4.34\%$, U_{ij} in Å².

Compared to the room temperature structure, the disorder scenario of the apical oxygen atoms is completely modified at 400 °C, evolving towards a double-well potential and strongly increasing the anharmonic displacements of the apical oxygen atoms. This is readily seen from the harmonic refinement only, by an increase of the U_{33} displacement parameter of O_{ap}, as listed in [Table 2](#). While Pr atoms as well show a significant deviation from harmonic displacements, those of the nickel and equatorial oxygen atoms remain merely unchanged.

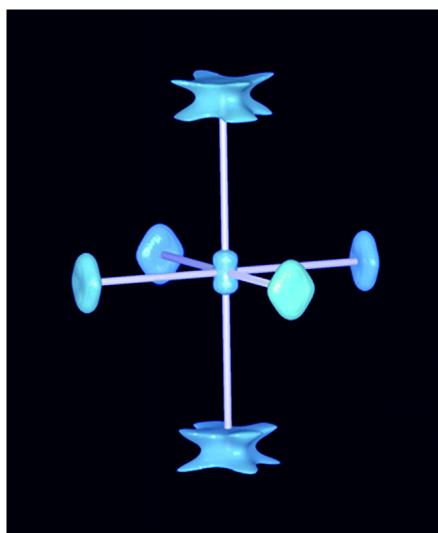


Fig. 4 Representation of the isosurfaces of the NiO_6 octahedron in $\text{Pr}_2\text{NiO}_{4.25}$, obtained from Maximum Entropy reconstruction of single crystal neutron diffraction data at 400 °C (HEiDi@MLZ, FRM II reactor in Garching).

As evidenced in Fig. 5, the outer parts of the O_{ap} displacements towards [110] become much more pronounced at 400 °C, pointing to a significant extent towards the interstitial sites, compared to what is found at ambient temperature. We therefore conclude on an almost steady overlap of a portion of the apical and interstitial oxygen sites as can be seen in Fig. 5, thereby establishing an oxygen diffusion pathway with a shallow potential. Concerning the equatorial oxygen atoms, one can figure out a more disk-like shaped scattering density perpendicular to the Ni–O bond.

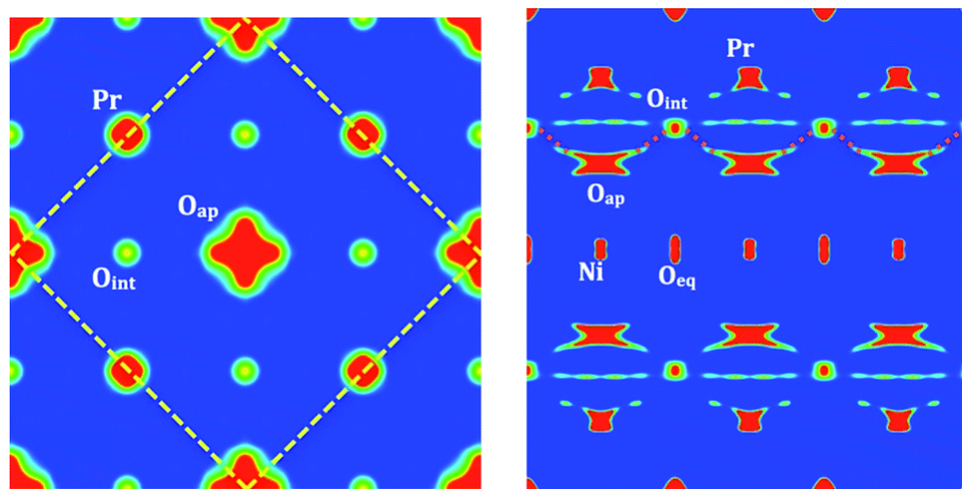


Fig. 5 Nuclear densities of PNO, obtained from neutron single crystal diffraction data via MEM analysis at 400 °C. Left part: $2a \times 2a$ projection of the $I4/mmm$ unit cell (the F -centred cell is outlined by yellow dashed bars) from $z = 0.12$ to $z = 0.28$ (upper), thus showing half of the rock salt layer with positions of Pr, apical oxygen and interstitial oxygen atoms at $z = 0.14$, 0.17 and 0.25 , respectively. Right part: $3a \times c$ projection from $y = 0.45$ to $y = 0.55$ of the I -cell. A dashed red line indicates the oxygen diffusion pathways along the [110]-direction in the F -cell (equivalent to [100] of the I -cell), between apical and interstitial sites.

The important anharmonic displacements experimentally evidenced by neutron diffraction nicely underline that dynamical aspects become important, transforming the Pr_2O_2 rock salt layer into a dynamically activated interface, where 2D oxygen diffusion takes place. Thus, it becomes clear that the potential of the apical oxygen atoms (as well as Pr atoms) can no longer be considered as harmonic, equally excluding the NiO_6 octahedra to be seen as a rigid unit. The direct observation of important anharmonic displacements also implies facile oxygen mobility at least on a local level. Anharmonic displacements, with respect to oxygen ion diffusion mechanisms, have also been found and simulated in apatite to occur at much higher temperatures.^{40,41} A double potential for the apical

oxygen atoms has also been reported for $\text{La}_{1.85}\text{Sr}_{0.15}\text{CuO}_4$ as determined by EXAFS, which has been interpreted as two conformations for the CuO_6 octahedra below 100 K.⁴² Strong anharmonic displacements have, as well, been discussed to explain the unusual increase in the self-diffusion coefficient around the bcc to hcp martensitic transitions of bcc metals as Hf and Ti but at high temperatures, far above 1000 °C.^{43–45} For this reason, this example does not seem to fit at first sight to the behaviour found in PNO at ambient temperature.

The temperature itself is, however, not supposed to be the essential parameter, as a similar scenario has also been found for the bcc/hcp phase transition in solid He below 2 K, with self-diffusion coefficients reaching $10^{-5} \text{ cm}^2 \text{ s}^{-1}$, corresponding to those found for liquids and which have been interpreted to be a consequence of the coupling of a vacancy to transverse phonons of short wavelength, softening at the phase transition.^{46,47} The fact that phonon assisted diffusion mechanisms are found even below 2 K strengthens the idea that similar mechanisms play an essential role in structurally anisotropic oxides and more specifically, those which can be considered as intergrowth phases, which might allow decoupling of dynamical behaviour of the different constituents. In the case of PNO, we might accordingly separate the NiO_2 layers from the Pr_2O_2 rock salt layer units, while the latter – at least from a dynamical point of view – approach the situation found for the bcc/hcp phase transitions reported above. The difference here is that the part of the structure becoming anharmonic is embedded in a matrix of NiO_2 layers, stabilizing the entire structural K_2NiF_4 -type framework. We note that this concept works in a similar way for Brownmillerites, where the high oxygen mobility in $\text{SrFeO}_{2.5}$, already present at ambient temperature, has been discussed to be the consequence of specific lattice dynamics, resulting from the dynamical decoupling of the $(\text{FeO}_4)_\infty$ tetrahedral chains from the rigid infinite square-planar FeO_2 layers. Here, the structural instability is generated by the O_{ap} atoms of the supposed FeO_6 octahedra, revealing sufficiently strong displacements from their equilibrium position to escape *in fine* into the vacancy channels of the tetrahedral layers on a ps timescale.^{17,18}

Consequently, we interpret the displacements found in PNO to be not only different from a classical description of harmonic Debye–Waller behaviour, but more importantly to rely on phonon coupling to interstitial oxygen atoms/vacancies, similar to what is observed for bcc/hcc phase transitions in metals or He as discussed above.

Even though anharmonic displacements for PNO at ambient temperature are less obvious than at 400 °C, it seems that a similar behaviour of the O_{ap} displacements is present at RT as can be seen in [Fig. 3](#). From the deformations coming out for the apical oxygen isosurfaces, a significant buckling along the *c*-direction is observed in addition to the displacements along [110], which do not develop in the same way for NNO. This might then account for the higher oxygen diffusion in the (*a*, *b*)-plane for PNO compared to NNO, associated with a much lower activation energy of 0.5 eV vs. 1.4 eV, respectively.³⁸

The double potential of the apical oxygen atoms is thus supposed to originate from the distortions/ordering generated from the interstitial oxygen atoms. We have to consider that each interstitial oxygen atom symmetrically increases the $(\text{O}_{\text{ap}})_4\text{O}_{\text{int}}$ tetrahedron, while O_{ap} atoms are strongly displaced away from their equilibrium position. Those O_{ap} atoms not directly involved in a $(\text{O}_{\text{ap}})_4\text{O}_{\text{int}}$ unit can, on the other hand, easily point towards the vacant interstitial sites. We note that only one out of eight interstitial sites gets occupied for a stoichiometry of $\text{Pr}_2\text{NiO}_{4.25}$. While the presence of interstitial oxygen atoms seems to be required to form the double potential, it is not yet clear on how the generation of anharmonic displacements depends on δ .

Two possible oxygen displacement scenarios for $\text{Pr}_2\text{NiO}_{4.25}$ are shown in [Fig. 6](#), where one extra oxygen atom is distributed over one F-type unit cell, containing overall $\text{Pr}_8\text{Ni}_4\text{O}_{17}$, *i.e.* 29 atoms.

Anharmonic apical oxygen displacements were not reported from the Maximum Entropy analysis for NPD of $(\text{Pr}_{0.9}\text{La}_{0.1})_2(\text{Ni}_{0.74}\text{Cu}_{0.21}\text{Ga}_{0.05})\text{O}_{4+\delta}$ at 1015 °C, as one might expect when compared to the results presented above for PNO at 400 °C. Possible reasons related to the resolution of the measured structure factors were collected up to a momentum transfer of only $\sin \vartheta/\lambda = 0.5 \text{ \AA}^{-1}$ in [ref. 37](#), while the present work takes into account single crystal neutron diffraction data up to $\sin \vartheta/\lambda = 0.89 \text{ \AA}^{-1}$. Another possibility could originate from the influence of the amount of interstitial oxygen atoms, since δ decreases to less than 0.15 above 1000 °C.⁴⁸ From the structure refinement of $(\text{Pr}_{0.9}\text{La}_{0.1})_2(\text{Ni}_{0.74}\text{Cu}_{0.21}\text{Ga}_{0.05})\text{O}_{4+\delta}$ at 1015 °C, a value of only $\delta = 0.026$ has been refined, while δ gets reduced to 0.20 at 400 °C for $\text{Pr}_2\text{NiO}_{4.23}$ as found by TGA.⁴⁸ It would therefore be extremely interesting to collect single crystal neutron data for the PNO crystal at 1000 °C.

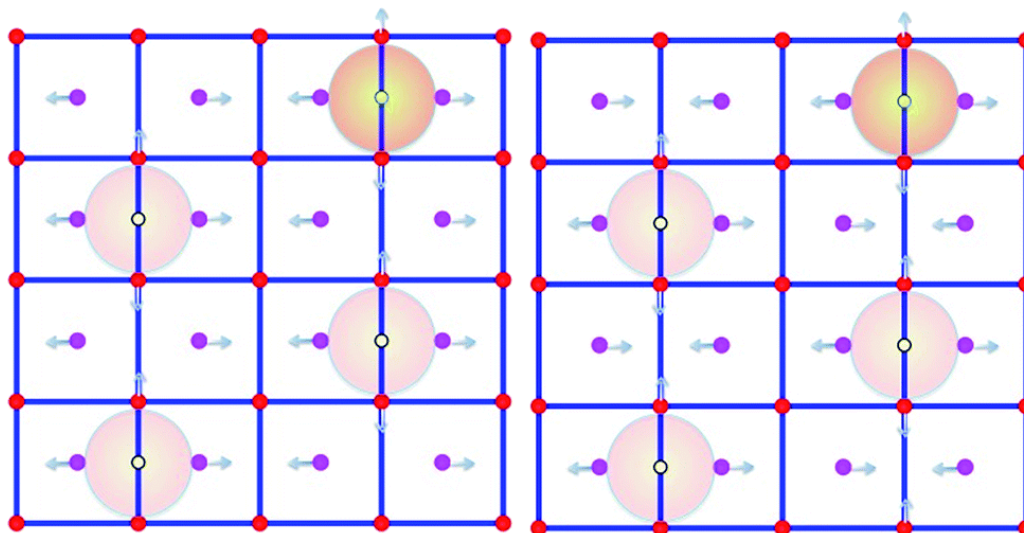


Fig. 6 Possible apical oxygen shift scenarios, taking into account an exact stoichiometry of PNO. Apical oxygen atoms of different heights (red: $z = 0.17$; magenta: $z = 0.33$) are indicated for one rock-salt type layer; a big yellow/reddish circle shows the steric influence of the interstitial atoms, displacements indicated by arrows. A 4×4 $I4/mmm$ unit cell is outlined in blue, the arrows pointing towards the $[110]$ direction of the F -cell.

It becomes thus obvious that, due to anharmonic displacements of the apical oxygen atoms, theoretical attempts to calculate and predict diffusion potentials become a difficult task, since a classical description becomes inappropriate. For example, using the Born model and Buckingham pair potentials in atomistic and molecular dynamics approaches becomes questionable and might be inaccurate to catch the apical oxygen dynamics. In this way it also becomes understandable that the strong anharmonic delocalization of the apical oxygen atoms accounts for the refined oxygen occupation, showing 15% deficiency as an artefact.

We interpret the driving force of the strong anharmonic potentials to rely, in addition to the presence of interstitial oxygen atoms, also on the quite short c -axis parameter of PNO and NNO ($c = 12.10 \text{ \AA}$ and 12.15 \AA , respectively, for the stoichiometric compounds), compared to much higher values found for $\text{La}_2(\text{Cu}/\text{Ni}/\text{Co})\text{O}_4$ and related K_2NiF_4 type oxides. The smaller ionic radii for Nd^{3+} and Pr^{3+} compared to La^{3+} result in an increased lattice mismatch and shortened $\text{RE}-\text{O}_{\text{ap}}$ bond, which, as a consequence, are supposed to push the apical oxygen atom away from their central position at $(0, 0, z)$. This may at least partially account for the excellent oxygen mobility especially for PNO and its promising properties as mixed ionic and electronic (MIEC) membranes for SOFCs.

Conclusion

High oxygen mobility in NNO and PNO, already present at room temperature, can be understood in terms of a dynamically activated interstitial diffusion mechanism. From single crystal neutron

diffraction data, large displacement amplitudes of the apical oxygen atoms along the [110]-direction of the F-centered unit cell have been revealed to be present at ambient temperature, getting amplified above 400 °C above the orthorhombic-tetragonal phase transition. The large displacement amplitudes of the apical oxygen atoms are discussed in regard to a similar behaviour found in bcc metals above 100 °C, as well as for solid He below 2 K, just before entering the bcc/fcc martensitic phase transition which is accompanied by an anomalous increase of the self-diffusion coefficient, strongly coupled to a phonon softening.

Consequently, the strong displacements promote phonon enhanced oxygen diffusion to proceed on a shallow potential diffusion pathway, between apical and interstitial lattice sites. Further on, a nearly coherent overlap between apical and interstitial oxygen sites above the phase transition has been evidenced from the nuclear scattering densities, as obtained from the Maximum Entropy reconstruction of single crystal neutron diffraction data up to high momentum transfers. The apical oxygen displacements in NNO/PNO are by far the strongest ever observed in K_2NiF_4 type frameworks, showing distortions of more than 1 Å from their equilibrium position at ambient temperature, which is equivalent to a tilt of the NiO_6 octahedra of more than 25°.

The anharmonic double potential of the apical oxygen as well as Pr atoms, established above the orthorhombic-tetragonal phase transition at 360 °C, clearly indicates a dynamic decoupling of the Pr_2O_2 rock salt layer from an embedding matrix of NiO_2 layers. This underlines the important role of lattice dynamics in contributing to an essentially 2D oxygen diffusion mechanism in the Pr_2O_2 rock salt layer, already at moderate temperatures. This is an important observation that underlines the limitations of classical approaches using inappropriate harmonic potentials to describe these anomalous anisotropic lattice dynamics.

Describing phonon-assisted diffusion in terms of the Arrhenius ansatz might then be a question on how the classical behaviour can be convoluted from isotropic to strongly anisotropic lattice dynamics, and to extend the Arrhenius formalism towards a tensor notation; this would then allow accounting for an anisotropic energy landscape and related activation energies for low temperature diffusion processes, with a strong directional approach.

The interstitial oxygen atoms play a predominant role in the oxygen diffusion mechanism, since they induce a strong delocalization of the apical oxygen atoms and deeply affect lattice dynamics. Since NNO and PNO still show an important amount of extra oxygen atoms at fairly elevated temperatures, *e.g.* $\delta \approx 0.15$ at around 1000 °C, this might then be the key reason why both title compounds are promising oxygen ion membranes to serve in SOFCs at intermediate temperatures.

In this regard it becomes also evident that the origin of the low temperature oxygen diffusion mechanism is related to the structural instability of the apical oxygen atoms, resulting from the HTT-LTO phase transition and associated phonon softening, allowing large dynamic apical oxygen displacements, promoting oxygen diffusion activated essentially by anharmonic lattice dynamics.

In the same way, one also understands that oxygen atoms are getting easily released from K_2NiF_4 type oxides, as in the case of La_2CuO_4 which forms the vacancy ordered $La_2CuO_{3.5}$ at temperatures as low as 200 °C when exposed to reducing agents such as CaH_2 .⁴⁹ In this context non-stoichiometric K_2NiF_4 -type oxides can therefore be considered as oxygen buffer compounds with interesting perspectives for technological applications.

Acknowledgements

The authors are grateful for financial support obtained through the ANR project AMOXIS (No. ANR-14-CE05-0016-02). We also acknowledge the use of neutron beam time on 5C2 at the Laboratoire Léon Brillouin (LLB) in Saclay (France), on RESI and HEiDI at the Forschungs-Neutronenquelle Heinz Maier-Leibnitz (FRM II) in Garching (Germany). HeiDI is operated by RWTH Aachen and Forschungszentrum Jülich *via* the JARA-FIT initiative.

References

1. Z. Shao , S. M. Haile , J. Ahn , P. D. Ronney , Z. Zhan and S. A. Barnett , *Nature*, 2005, **435** , 795 —798.
2. Z. Shao and S. M. Haile , *Nature*, 2004, **431** , 170 —173.
3. N. Q. Minh *J. Am. Ceram. Soc.*, 1993, **76** , 563 —588.
4. Y.-H. Huang , R. I. Dass , Z.-L. Xing and J. B. Goodenough , *Science*, 2006, **312** , 254 —257.
5. A. Atkinson , S. Barnett , R. J. Gorte , J. T. S. Irvine , A. J. McEvoy , M. Mogensen , S. C. Singhal and J. Vohs , *Nat. Mater.*, 2004, **3** , 17 —27.
6. P. Rudolf , W. Paulus and R. Schöllhorn , *Adv. Mater.*, 1991, **3** , 438 —440.
7. W. Paulus , G. Heger , P. Rudolf and R. Schöllhorn , *Phys. C*, 1994, **235–240** , 861 —862.
8. W. Paulus , A. Cousson , G. Dhalenne , J. Berthon , A. Revcolevschi , S. Hosoya , W. Treutmann , G. Heger and R. le Toquin , *Solid State Sci.*, 2002, **4** , 565 —573.
9. J. A. Alonso , M. J. Martínez-Lope , J. L. García-Muñoz and M. T. Fernández-Díaz , *J. Phys.: Condens. Matter*, 1997, **9** , 6417.
10. N. Gauquelin , T. E. Weirich , M. Ceretti , W. Paulus and M. Schroeder , *Monatshefte für Chemie*, 2009, **140** , 1095 —1102.
11. Y. Takeda , R. Kanno , T. Takada , O. Yamamoto , M. Takano and Y. Bando , *Zeitschrift für anorganische und allgemeine Chemie*, 1986, **540** , 259 —270.
12. A. Nemudry , M. Weiss , I. Gainutdinov , V. Boldyrev and R. Schöllhorn , *Chem. Mater.*, 1998, **10** , 2403 —2411.
13. A. Nemudry , P. Rudolf and R. Schöllhorn , *Chem. Mater.*, 1996, **8** , 2232 —2238.
14. A. Piovano , G. Agostini , A. I. Frenkel , T. Bertier , C. Prestipino , M. Ceretti , W. Paulus and C. Lamberti , *J. Phys. Chem. C*, 2010, **115** , 1311 —1322.
15. R. le Toquin , W. Paulus , A. Cousson , C. Prestipino and C. Lamberti , *J. Am. Chem. Soc.*, 2006, **128** , 13161 —13174.
16. S. Bhavaraju , J. F. DiCarlo , D. P. Scarfe , I. Yazdi and A. J. Jacobson , *Chem. Mater.*, 1994, **6** , 2172 —2176.
17. W. Paulus , H. Schober , S. Eibl , M. Johnson , T. Berthier , O. Hernandez , M. Ceretti , M. Plazanet , K. Conder and C. Lamberti , *J. Am. Chem. Soc.*, 2008, **130** , 16080 —16085.
18. A. Villesuzanne , W. Paulus , A. Cousson , S. Hosoya , L. le Dréau , O. Hernandez , C. Prestipino , M. Ikbel Houchati and J. Schefer , *J. Solid State Electrochem.*, 2011, **15** , 357 —366.
19. A. Nemudry , P. Rudolf and R. Schöllhorn , *Solid State Ionics*, 1998, **109** , 213 —222.
20. J. D. Sullivan , D. J. Buttrey , D. E. Cox and J. Hriljac , *J. Solid State Chem.*, 1991, **94** , 337 —351.
21. L. L. Dreau , PhD thesis, Université Rennes 1, 2011.
22. M. T. Fernández-Díaz , J. L. Martínez and J. Rodríguez-Carvajal , *Solid State Ionics*, 1993, **63–65** , 902 —906.
23. A. Perrichon , A. Piovano , M. Boehm , M. Zbiri , M. Johnson , H. Schober , M. Ceretti and W. Paulus , *J. Phys. Chem. C*, 2015, **119** , 1557 —1564.

24. O. Wahyudi , M. Ceretti , I. Weill , A. Cousson , F. Weill , M. Meven , A. Villesuzanne , M. Guerre , J.-M. Bassat and W. Paulus , *CrystEngComm*, 2015, **17** , 6278 —6285.
25. G. Sheldrick *Acta Crystallogr., Sect. A: Found. Crystallogr.*, 2008, **64** , 112 —122.
26. R. A. D. F. Izumi *Recent Research Developments in Physics* , 2002.
27. L. Koester *Neutron Physics* , Springer Berlin Heidelberg, 1977, vol. vol. 80, pp. 1–55.
28. K. Momma and F. Izumi , *J. Appl. Crystallogr.*, 2011, **44** , 1272 —1276.
29. L. le Dréau , C. Prestipino , O. Hernandez , J. Schefer , G. Vaughan , S. Paofai , J. M. Perez-Mato , S. Hosoya and W. Paulus , *Inorg. Chem.*, 2012, **51** , 9789 —9798.
30. R. le Toquin , W. Paulus , A. Cousson , G. Dhalenne and A. Revcolevschi , *Phys. B*, 2004, **350** , E269 —E272.
31. P. Schiebel , K. Wulf , W. Prandl , G. Heger , R. Papoular and W. Paulus , *Acta Crystallogr., Sect. A: Found. Crystallogr.*, 1996, **52** , 176 —188.
32. L. Minervini , R. W. Grimes , J. A. Kilner and K. E. Sickafus , *J. Mater. Chem.*, 2000, **10** , 2349 —2354.
33. R. D. Shannon and C. T. Prewitt , *Acta Crystallogr., Sect. B: Struct. Crystallogr. Cryst. Chem.*, 1969, **25** , 925 —946.
34. J. D. Jorgensen , B. Dabrowski , S. Pei , D. R. Richards and D. G. Hinks , *Phys. Rev. B: Condens. Matter Mater. Phys.*, 1989, **40** , 2187 —2199.
35. C. Frayret , A. Villesuzanne and M. Pouchard , *Chem. Mater.*, 2005, **17** , 6538 —6544.
36. D. Parfitt , A. Chroneos , J. A. Kilner and R. W. Grimes , *Phys. Chem. Chem. Phys.*, 2010, **12** , 6834 —6836.
37. M. Yashima , M. Enoki , T. Wakita , R. Ali , Y. Matsushita , F. Izumi and T. Ishihara , *J. Am. Chem. Soc.*, 2008, **130** , 2762 —2763.
38. J.-M. Bassat , M. Burriel , O. Wahyudi , R. Castaing , M. Ceretti , P. Veber , I. Weill , A. Villesuzanne , J.-C. Grenier , W. Paulus and J. A. Kilner , *J. Phys. Chem. C*, 2013, **117** , 26466 —26472.
39. M. T. Fernández-Díaz , J. Rodríguez-Carvajal , J. L. Martínez , G. Fillion , F. Fernández and R. Saez-Puche , *Zeitschrift für Physik B Condensed Matter*, 1991, **82** , 275 —282.
40. K. Fukuda , T. Asaka , M. Oyabu , D. Urushihara , A. Berghout , E. Béchade , O. Masson , I. Julien and P. Thomas , *Chem. Mater.*, 2012, **24** , 4623 —4631.
41. E. Kendrick , M. S. Islam and P. R. Slater , *J. Mater. Chem.*, 2007, **17** , 3104 —3111.
42. A. Bianconi , N. L. Saini , A. Lanzara , M. Missori , T. Rossetti , H. Oyanagi , H. Yamaguchi , K. Oka and T. Ito , *Phys. Rev. Lett.*, 1996, **76** , 3412 —3415.
43. W. Petry , A. Heiming , J. Trampenau , M. Alba , C. Herzig , H. R. Schober and G. Vogl , *Phys. Rev. B: Condens. Matter Mater. Phys.*, 1991, **43** , 10933 —10947.
44. A. Heiming , W. Petry , J. Trampenau , M. Alba , C. Herzig , H. R. Schober and G. Vogl , *Phys. Rev. B: Condens. Matter Mater. Phys.*, 1991, **43** , 10948 —10962.
45. J. Trampenau , A. Heiming , W. Petry , M. Alba , C. Herzig , W. Miekeley and H. R. Schober , *Phys. Rev. B: Condens. Matter Mater. Phys.*, 1991, **43** , 10963 —10969.
46. I. Berent and E. Polturak , *J. Low Temp. Phys.*, 1998, **112** , 337 —354.
47. T. Markovich , E. Polturak , S. G. Lipson , J. Bossy , E. Farhi , M. J. Harris and M. J. Bull , *J. Low Temp. Phys.*, 2002, **129** , 65 —77.
48. C. Allancon , J. Rodríguez-Carvajal , M. T. Fernández-Díaz , P. Odier , J. M. Bassat , J. P. Loup and J. L. Martínez , *Zeitschrift für Physik B Condensed Matter*, 1996, **100** , 85 —90.
49. M. I. Houchati , M. Ceretti , C. Ritter and W. Paulus , *Chem. Mater.*, 2012, **24** , 3811 —3815.